Discovery of a vezatin-like protein for dynein-mediated early endosome transport

Xuanli Yao[a], Herbert N. Arst, Jr.[b], Xiangfeng Wang[c,*], and Xin Xiang[a]
[a]Department of Biochemistry and Molecular Biology, Uniformed Services University of the Health Sciences–F. Edward Hébert School of Medicine, Bethesda, MD 20814; [b]Microbiology Section, Department of Medicine, Imperial College London, London SW7 2AZ, United Kingdom; [c]School of Plant Sciences, University of Arizona, Tucson, AZ 85721

ABSTRACT **Early endosomes are transported bidirectionally by cytoplasmic dynein and kinesin-3, but how the movements are regulated in vivo remains unclear. Here our forward genetic study led to the discovery of VezA, a vezatin-like protein in *Aspergillus nidulans*, as a factor critical for early endosome distribution. Loss of *vezA* causes an abnormal accumulation of early endosomes at the hyphal tip, where microtubule plus ends are located. This abnormal accumulation depends on kinesin-3 and is due to a decrease in the frequency but not the speed of dynein-mediated early endosome movement. VezA-GFP signals are enriched at the hypha tip in an actin-dependent manner but are not obviously associated with early endosomes, thus differing from the early endosome association of the cargo adapter HookA (Hook in *A. nidulans*). On loss of VezA, HookA associates normally with early endosomes, but the interaction between dynein-dynactin and the early-endosome-bound HookA is significantly decreased. However, VezA is not required for linking dynein-dynactin to the cytosolic ΔC-HookA, lacking the cargo-binding C-terminus. These results identify VezA as a novel regulator required for the interaction between dynein and the Hook-bound early endosomes in vivo.**

Monitoring Editor
Xueliang Zhu
Chinese Academy of Sciences

Received: Aug 27, 2015
Revised: Sep 4, 2015
Accepted: Sep 6, 2015

INTRODUCTION

The minus end–directed cytoplasmic dynein motor transports organelles/vesicles and proteins/mRNA along microtubules, and its function is important for many cellular processes in both lower and higher eukaryotes (Kardon and Vale, 2009; Perlson *et al.*, 2010; Vallee *et al.*, 2012). However, mechanistically how dynein-mediated transport is regulated in vivo is unclear; in particular, we do not fully understand how dynein interacts with its various cargoes and how its activity is coordinated with that of plus end–directed kinesins (Akhmanova and Hammer, 2010; Fu and Holzbaur, 2014). Several important dynein regulators have been identified, including the dynactin complex, LIS1, and NudE/Nudel (Schroer, 2004; Kardon and Vale, 2009; Vallee *et al.*, 2012), and the functional connection between dynein and LIS1 and that between LIS1 and NudE/Nudel were first suggested by genetic data obtained in the filamentous fungus *Aspergillus nidulans* (Xiang *et al.*, 1995a; Efimov and Morris, 2000). Although mechanistic studies of these known regulators are critical for our understanding of dynein regulation, identification of novel factors required for dynein-mediated transport in vivo also represents an important complementary approach.

Filamentous fungi are well suited for studying dynein-mediated transport of early endosomes (Granger *et al.*, 2014; Steinberg, 2014; Xiang *et al.*, 2015). As first discovered in *Ustilago maydis*, the microtubule plus end–directed kinesin-3 moves early endosomes toward the plus end, and dynein moves them away from the plus end (Wedlich-Soldner *et al.*, 2002; Lenz *et al.*, 2006; Abenza *et al.*, 2009; Zekert and Fischer, 2009; Egan *et al.*, 2012). In *A. nidulans*, dynein accumulates at the microtubule plus end near the hyphal tip, and this localization requires kinesin-1 as well as dynactin (Han *et al.*, 2001; Zhang *et al.*, 2003; Egan *et al.*, 2012; Yao *et al.*, 2012). The plus-end accumulation of dynein facilitates transport of early endosomes toward the minus end, most likely by enhancing the chance of dynein–early endosome interaction (Lenz *et al.*, 2006; Zhang *et al.*, 2010; Schuster *et al.*, 2011a,b) and/or possibly by

This article was published online ahead of print in MBoC in Press (http://www.molbiolcell.org/cgi/doi/10.1091/mbc.E15-08-0602) on September 16, 2015.

*Present Address: Department of Plant Genetics and Breeding, College of Agronomy and Biotechnology, China Agricultural University, Beijing 100193, China.

Address correspondence to: Xin Xiang (xin.xiang@usuhs.edu).

Abbreviations used: DMSO, dimethyl sulfoxide; GFP, green fluorescent protein; HC, heavy chain.

allowing the interaction to occur at the hyphal tip region where a positive regulator may be located. The association between dynein and early endosomes requires the dynactin complex, particularly the β-helix–containing p25 subunit (Eckley *et al.*, 1999; Zhang *et al.*, 2011; Yeh *et al.*, 2013), which is not required for nuclear distribution (as first shown in *Neurospora crassa*) but is required for early endosome transport in both *A. nidulans* and mammalian cells (Lee *et al.*, 2001; Zhang *et al.*, 2011; Yeh *et al.*, 2012). Recently genetic screens in *A. nidulans* and *U. maydis* led to the discovery of the Hook-FTS-FHIP complex, a complex first found in higher eukaryotes (Kramer and Phistry, 1996; Xu *et al.*, 2008), as critical for linking dynein-dynactin to early endosomes, and *U. maydis* Hook (Hok1) also plays an important role in recruiting kinesin-3 to these cargoes (Bielska *et al.*, 2014; Yao *et al.*, 2014; Zhang *et al.*, 2014). However, it has not been clear whether additional factors are required for regulating the bidirectional transport of early endosomes.

Here we report the identification of a novel factor, vezatin-like protein in *A. nidulans* (VezA), which is critical for dynein-mediated early endosome transport. VezA contains a vezatin domain, as well as two predicted transmembrane domains similar to those in the mammalian vezatin protein. Vezatin is involved in neuronal functions, stabilization of cell–cell adhesion, and *Listeria* entry into cells, and it is also a putative tumor suppressor and linked with endometriosis (Kussel-Andermann *et al.*, 2000; Sousa *et al.*, 2004; Bahloul *et al.*, 2009; Sanda *et al.*, 2010; Danglot *et al.*, 2012; Miao *et al.*, 2013; Pagliardini *et al.*, 2015). Vezatin interacts with FERM domain–containing proteins (Kussel-Andermann *et al.*, 2000; Bahloul *et al.*, 2009), and it also interacts specifically with the GTP-bound ADP-ribosylation factor 6, Arf6 (Sanda *et al.*, 2010). Although the mammalian vezatin proteins have never been implicated in microtubule-based transport, loss of VezA in *A. nidulans* causes an obvious defect in dynein-mediated transport of early endosomes. Of interest, VezA is enriched at the hyphal tip but does not appear to colocalize with early endosomes, which is in contrast to HookA (Hook in *A. nidulans*), which is obviously associated with early endosomes. Of importance, although VezA does not affect HookA–early endosome association, it affects the interaction between dynein and HookA when HookA is attached to the early endosome. Thus VezA is a novel factor regulating dynein–early endosome interaction in vivo.

RESULTS

Identifying VezA as a novel factor required for early endosome distribution

We ultraviolet (UV)-mutagenized *A. nidulans* conidiospores and screened for early endosome distribution (*eed*) mutants, which exhibit an abnormal accumulation of early endosomes at the hyphal tip. Because mutations that affect the overall function of dynein severely inhibit colony growth but mutants that are more specifically defective in early endosome movement form relatively healthy colonies (Zhang *et al.*, 2011, 2014), we selected the mutants that formed relatively healthy colonies. Moreover, to limit the chance of finding genes that affect the general function or localization of dynein, we collected only those mutants in which dynein localization at the microtubule plus ends can be seen and dynein-mediated nuclear distribution appears normal. Previous screens allowed us to identify the *eedA* and *eedB* genes, which encode HookA and FhipA, respectively (Yao *et al.*, 2014; Zhang *et al.*, 2014). In the present study, we selected a mutant, *eed*27, whose colonies appear slightly more compact than that of the wild type (Figure 1A), but whose colony phenotype is even subtler than that of the Δ*fhipA* or Δ*hookA* mutant. Microscopic observations of the *eed*27 mutant revealed an abnormal accumulation of early endosomes at a vast majority of hyphal tips (>80%, $n > 100$; Figure 1, B and C, and Supplemental Movies S1 and S2), whereas plus-end comets of dynein are present (Figure 1B). Despite the abnormal accumulation at the hyphal tip in the mutant, mCherry-RabA (Rab5 homologue)–labeled early endosomes can be seen moving in both directions (Figure 1C), which differs from the Δ*hookA* mutant, in which we almost never observed movement. To determine whether the newly identified *eed*27 mutation is in the previously identified genes involved in dynein-mediated early endosome transport but not in the overall function of dynein, for example, p25 of dynactin, *hookA*, or *fhipA*, we crossed the *eed*27 mutant with the Δp25, Δ*hookA*, or Δ*fhipA* mutant. All of these crosses generated wild-type progeny, indicating that the *eed*27 mutation is not in any of these known genes, and thus we named the mutation *eedC27*.

To identify the *eedC*27 mutation, we used a combination of classical genetic and whole-genome sequencing approaches. Whole-genome sequencing was done using the genome sequencing and bioinformatic service of Otogenetics (www.otogenetics.com). We also used the software Tablet (version 1.13.12.17, James Hutton Institute; ics.hutton.ac.uk/tablet/download-tablet/tablet-release-notes/) for visualizing sequence assemblies and alignments (Milne *et al.*, 2013). To facilitate gene identification, we used the parasexual cycle of *A. nidulans* to map the *eedC*27 mutation to chromosome VIII, and this combination of genetic and genome-sequencing approaches allowed us to identify the gene without any ambiguity. The *eedC* gene corresponds to An10076, which encodes a novel protein with 615 amino acids. Of interest, the protein contains a vezatin domain (amino acids [aa] ~150–380; Figure 1D) and shows weak similarity to the mammalian vezatin, which was initially identified as a protein binding to the FERM domain of myosin VIIA to bring it close to the cadherin–catenin complex (Kussel-Andermann *et al.*, 2000; Supplemental Figure S1). Two transmembrane domains, aa 142–164 and 177–195, were predicted by the SMART program (smart.embl-heidelberg.de/; Figure 1D and Supplemental Figure S1). Note that the mammalian vezatin also contains two transmembrane domains (aa 134–158 and 166–188; Bahloul *et al.*, 2009). The *eedC*27 mutation is a deletion of a nucleotide T, creating a frameshift after aa 276. Because of the sequence similarity to vezatin, we named the *eedC* gene *vezA* and the encoded protein VezA.

To confirm that VezA is required for early endosome distribution, we made the deletion mutant Δ*vezA* (Supplemental Figure S2), and performed a detailed analysis on its phenotype. The Δ*vezA* mutant showed a colony phenotype nearly identical to that of the original UV-generated *eedC*27 mutant (Figure 2A). Just like the original mutant, the Δ*vezA* mutant also exhibited an abnormal accumulation of mCherry-RabA–labeled early endosomes at the hyphal tip (Figure 2B). Dynein comets, which represent the microtubule plus-end accumulation of dynein, were present (Figure 2B). In addition, Δ*vezA* exhibited a normal pattern of nuclear distribution (Figure 2C). Taken together, these results indicate that VezA is not essential for the overall function and localization of dynein but is critical for dynein-mediated early endosome transport.

To determine whether VezA functions solely in a genetic pathway with HookA or p25, we constructed Δ*vezA* Δ*hookA* and Δ*vezA* Δp25 double mutants. Of interest, the Δ*vezA* Δ*hookA* and Δ*vezA* Δp25 double-mutant colonies looked slightly more compact than the Δ*hookA* or Δp25 single mutants, respectively (Supplemental Figure S2C), suggesting that VezA might participate in additional pathways beyond that of the p25/HookA–controlled early endosome transport.

Endocytosis in fungi involves actin patches (Engqvist-Goldstein and Drubin, 2003; Gachet and Hyams, 2005; Michelot *et al.*, 2010;

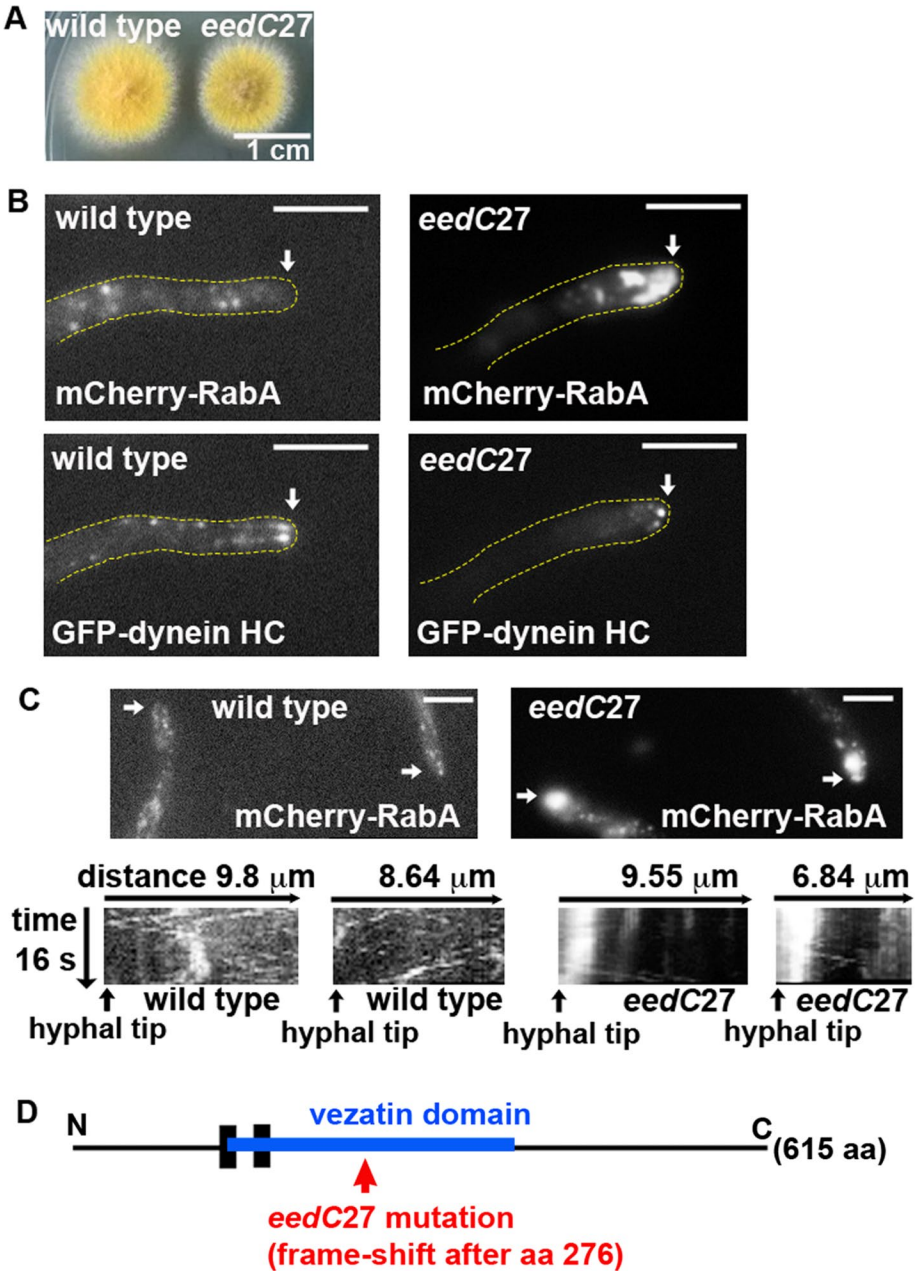

FIGURE 1: Phenotype of the *eedC27* mutant and the position of the *eedC*27 mutation in VezA. (A) Colony phenotypes of a wild-type strain and the *eedC27* mutant. (B) Microscopic images showing the distributions of mCherry-RabA–labeled early endosomes (mCherry-RabA) and GFP-labeled dynein heavy chain (GFP-HC). The same cells are shown for both the mCherry-RabA and GFP-HC images. Dynein comets are present in both wild-type and mutant hyphae. Yellow dotted lines show the hyphal shape. Arrows indicate the positions of the hyphal tips. Bars, 5 μm. (C) Microscopic images and kymographs showing the distributions of mCherry-RabA–labeled early endosomes (mCherry-RabA) in the wild type and the *eedC*27 mutant. Arrows indicate the positions of the hyphal tips. Diagonal lines in kymographs indicate movements of early endosomes. Bars, 5 μm. Supplemental Movies S1 and S2 are related to this figure. (D) A diagram showing positions of the vezatin domain and the *eedC*27 mutation of VezA. The two predicted transmembrane domains are shown as vertical black bars.

Sirotkin *et al.*, 2010; Basu and Chang, 2011; Mooren *et al.*, 2012), and the endocytosis machinery in *A. nidulans* and other filamentous fungi has been observed to localize preferentially at a collar right behind the hyphal tip, suggesting that hyphal tip growth and endocytosis are tightly coupled (Araujo-Bazan *et al.*, 2008; Taheri-Talesh *et al.*, 2008; Upadhyay and Shaw, 2008; Peñalva, 2010; Echauri-Espinosa *et al.*, 2012). However, endocytosis along the whole hyphae, as evidenced by uptake of the dye FM4-64, has been observed to occur in live cells (Peñalva, 2005). The newly formed endocytic vesicles would fuse with Rab5 (RabA and RabB of *A. nidulans*)–positive early endosomes, and, as first shown in *U. maydis* (Wedlich-Soldner *et al.*, 2002; Lenz *et al.*, 2006), they would be transported toward the microtubule plus end by kinesin-3 before being moved back by dynein (Abenza *et al.*, 2009, 2010; Zekert and Fischer, 2009; Egan *et al.*, 2012).

Unlike Δ*hookA*, in which motile early endosomes were almost never observed, we were able to detect some motile early endosomes in the Δ*vezA* mutant (Figure 2D). We did a quantitative analysis of early endosome movement within a region ~5 μm from the hyphal tip where microtubule plus ends all face the hyphal tip (Xiang *et al.*, 2015). We found that the frequency of dynein-mediated movements (away from the hyphal tip) significantly decreased upon loss of VezA. The frequency of movements to the hyphal tip (kinesin-3 mediated) also decreased, which is similar to the situation in the Δp25 mutant (Figure 2E; Zhang *et al.*, 2011). To determine whether the hyphal-tip accumulation of early endosomes in the Δ*vezA* mutant is due to a defect in dynein motor activity, we also measured the speed of dynein-mediated early endosome movement. We found that the speed is clearly not reduced (Figure 2F), indicating that VezA does not affect dynein motor activity. To determine directly whether the abnormal hyphal-tip accumulation of early endosomes in the Δ*vezA* mutant depends on kinesin-3, we introduced the Δ*uncA* (kinesin-3) allele (Zekert and Fischer 2009) into the strain containing the Δ*vezA* allele. In the Δ*vezA* Δ*uncA* double mutant, the hyphal-tip accumulation of early endosomes in the Δ*vezA* single mutant was no longer observed (Figure 3A), and our quantitation of the hyphal-tip mCherry-RabA signals in the Δ*vezA* Δ*uncA* double mutant is consistent with a much reduced accumulation of early endosomes at the hyphal tip compared with that in the Δ*vezA* single mutant (Figure 3, A and B). These results indicate that VezA is involved in dynein-mediated early endosome transport after early endosomes are moved toward the hyphal tip by kinesin-3.

VezA proteins are enriched at the hyphal tip in an actin-dependent manner

To localize VezA, we constructed a strain in which the endogenous *vezA* gene is replaced by the *vezA*–green fluorescent protein (GFP) fusion gene (Supplemental Figure S3A). For comparison, we also

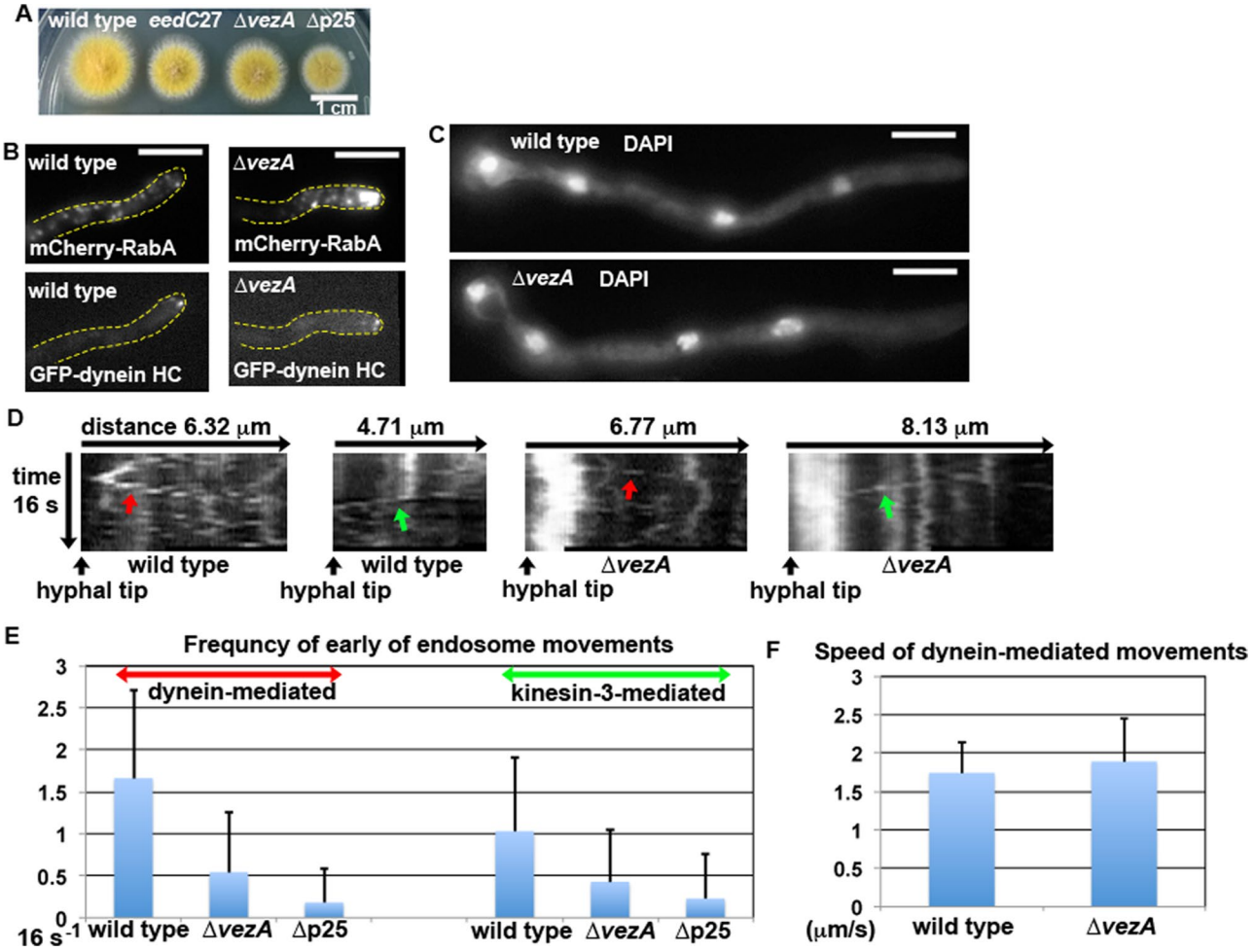

FIGURE 2: Functional analyses of VezA. (A) Colony phenotype of the Δ*vezA* mutant in comparison to that of a wild type, the original *eedC27* mutant, and the Δp25 mutant. (B) Distributions of mCherry-RabA–labeled early endosomes in the wild type and the Δ*vezA* mutant, and GFP-dynein HC (GFP-HC) signals in the same wild-type and the Δ*vezA* mutant cells. Yellow dotted lines show the hyphal shape. Bars, 5 μm. (C) Images of nuclei stained by DAPI in the wild type and the Δ*vezA* mutant. Bars, 5 μm. (D) Kymographs showing mCherry-RabA signals (diagonal lines indicating movements of early endosomes). Red arrows indicate dynein-mediated movements away from the hyphal tip. Green arrows indicate kinesin-3–mediated movements to the hyphal tip. (E) A quantitative analysis of the frequency of early endosome movements mediated by dynein or kinesin-3 within 16 s. For dynein-mediated movements, the mean ± SD values are 1.66 ± 1.05 for wild type ($n = 38$), 0.54 ± 0.72 for Δ*vezA* ($n = 61$), and 0.18 ± 0.40 for Δp25 ($n = 22$). The mean value of the Δ*vezA* mutant is significantly lower than that of the wild type ($p < 0.001$) but higher than that of the Δp25 ($p < 0.05$). For kinesin-3–mediated movements, the mean ± SD values are 1.03 ± 0.89 for wild type ($n = 38$), 0.43 ± 0.62 for Δ*vezA* ($n = 61$), and 0.23 ± 0.53 for Δp25 ($n = 22$). The mean value of the Δ*vezA* mutant is significantly lower than that of the wild type ($p < 0.001$) but not significantly different from that of the Δp25 at $p = 0.05$. (F) Quantitative analysis of the speed of early endosome movements mediated by dynein. The mean ± SD values are 1.74 ± 0.40 μm/s for wild type ($n = 19$) and 1.89 ± 0.56 μm/s for Δ*vezA* ($n = 22$). The mean value of the Δ*vezA* mutant is not significantly different from that of the wild type at $p = 0.05$.

constructed a strain in which the endogenous *vezA* gene is replaced by the ΔTM-*vezA*-GFP fusion gene missing the two predicted transmembrane domains (Supplemental Figure S3B). The VezA-GFP protein is functional, as cells expressing it exhibited a normal pattern of early endosome distribution (Figure 4A and Supplemental Movies S3 and S4). In contrast, the ΔTM-*vezA*-GFP strain exhibited a clear defect in early endosome distribution, as similarly exhibited by the Δ*vezA* mutant (Figure 4A and Supplemental Movie S5). VezA-GFP signals were significantly enriched at the hyphal tip in many cells (Figure 4B; Supplemental Movies S6–S8 show different examples). To visualize the plasma membrane, we stained the cells with FM4-64, a lipophilic dye that reveals the fungal plasma membrane if the cells are treated briefly (Galindo *et al.*, 2012; Kilaru *et al.*, 2015). However, the FM4-64 treatment seemed to disturb the hyphal-tip GFP signals, and thus we took the images of VezA-GFP before adding the dye and then took the FM4-64 images. In some of these cells, we saw a bright, dot-like GFP signal very close to the hyphal apex (Figure 4B). This dot-like signal seemed relatively stable (as shown in the kymograph in Figure 4B and in Supplemental Movie S6), but sometimes it was seen to move around (Supplemental Movie S7). Slightly behind it were VezA-GFP signals that were more dynamic but seemed to only undergo short-distance movements

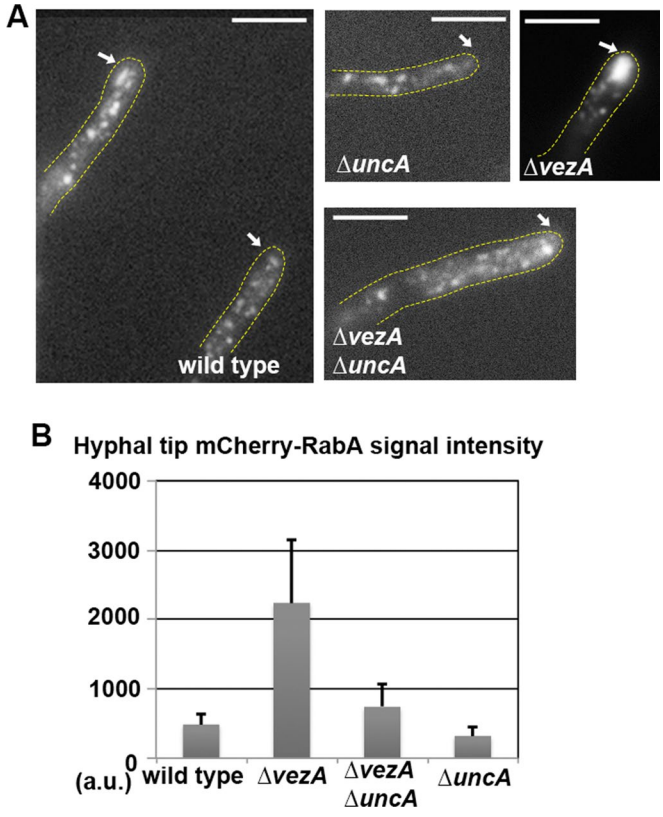

FIGURE 3: Phenotypic analyses of the Δ*vezA* Δ*uncA* (kinesin-3) double mutant. (A) Distribution of mCherry-RabA–labeled early endosomes in the Δ*vezA* Δ*uncA* double mutant in comparison to that in the wild type and the Δ*uncA* and Δ*vezA* single mutants. Yellow dotted lines show the hyphal shape. Arrows indicate the hyphal tip. Bars, 5 μm. (B) Quantitative analysis of the mean intensity values of mCherry-RabA signals within 2 μm behind the hyphal apex. The mean ± SD values are 483 ± 152 (arbitrary units [a.u.]) for wild type ($n = 10$), 2237 ± 902 for Δ*vezA* ($n = 12$), 736 ± 334 for Δ*vezA* Δ*uncA* ($n = 11$), and 318 ± 141 for Δ*uncA* ($n = 10$). The mean value of the Δ*vezA* Δ*uncA* double mutant is significantly lower than that of the Δ*vezA* single mutant ($p < 0.001$) and higher than that of the Δ*uncA* single mutant ($p < 0.05$) but not significantly different from that of the wild type at $p = 0.05$.

(Figure 4B and Supplemental Movies S6–S8). In contrast, the ΔTM-VezA-GFP signals were diffuse and not enriched at the hyphal tip (Figure 4C). Our Western analysis showed that the ΔTM-VezA-GFP protein is stable (Figure 4C), although we cannot completely rule out the possibility that the protein may not fold properly. To confirm this localization pattern of VezA, we constructed a strain expressing VezA fused with GFP at its N-terminus (GFP-VezA). In this strain, the GFP-*vezA* fusion gene also integrated into the *vezA* locus, and its expression is controlled by the *gpdA*^{mini} promoter (Pantazopoulou and Peñalva, 2009; Supplemental Figure S3C). The GFP-VezA fusion protein is also functional, as cells expressing it as the only source of VezA exhibited a normal pattern of early endosome distribution (Figure 4D). The signals of GFP-VezA were also enriched at the hyphal tip, similar to those of VezA-GFP. The localization pattern of VezA clearly differs from that of early endosomes in wild-type cells. Moreover, in the Δ*hookA* mutant with abnormally accumulated early endosomes, we could hardly detect any enrichment of VezA-GFP signals at the clusters of mCherry-RabA signals (Figure 4, E and F).

We next determined whether the hyphal-tip enrichment of VezA depends on microtubules or the actin cytoskeleton by using benomyl, a microtubule-depolymerizing drug, or latrunculin B, an actin polymerization inhibitor, respectively. Microtubules are not essential for polarized growth but are required for rapid hyphal elongation (Horio and Oakley, 2005), and, thus, short hyphae were seen after overnight treatment with benomyl at a concentration (1.2 μg/ml) that depolymerized all microtubules (unpublished data). Although the shapes of the hyphal tips looked less focused in benomyl-treated cells than in untreated cells, the hyphal-tip enrichment of VezA-GFP signals was still present (Figure 4G). In contrast, because actin polymerization is essential for polarized growth, we treated the VezA-GFP–containing cells with latrunculin B for only 15 min. Of interest, the VezA-GFP signals were quickly dispersed and the hyphal-tip enrichment was no longer observed after the treatment (Figure 4H), suggesting that the hyphal-tip localization of VezA is supported by the actin cytoskeleton. We would add a note of caution, however; because the hyphal-tip VezA-GFP signals also seemed to be perturbed by FM4-64 treatment, it is possible that they represent VezA localization to membranous structures that are partially tethered by the actin cytoskeleton.

VezA does not affect HookA–early endosome association but affects the interaction between early endosome–bound HookA and dynein-dynactin

As recently discovered in *A. nidulans* and *U. maydis*, Hook proteins link dynein to early endosomes, and in *A. nidulans*, HookA interacts with early endosomes via FhipA and FtsA (Bielska *et al.*, 2014; Yao *et al.*, 2014; Zhang *et al.*, 2014). To determine whether VezA affects HookA–early endosome association, we introduced the HookA-GFP fusion into the Δ*vezA* mutant by genetic crossing. We found that HookA-GFP proteins largely colocalize with mCherry-RabA–labeled early endosomes accumulated at the hyphal tip and individual early endosomes along the hypha (Figure 5A). To compare quantitatively the early endosome–associated HookA-GFP signals in the Δ*vezA* mutant and wild type, we treated wild-type and Δ*vezA* cells with benomyl overnight, which allowed us to measure the ratio of HookA-GFP to mCherry-RabA on early endosomes that are not clustered together at the hyphal tip. Our analysis showed that the values from the wild type and the mutant were nearly identical, indicating that VezA does not affect the association between HookA and early endosomes (Figure 5, B and C).

We next determined whether VezA affects the ability of HookA to interact with dynein, using biochemical pull-down assays. For this experiment, we first introduced the ΔC-HookA-GFP fusion into the Δ*vezA* mutant by genetic crossing. As shown previously, HookA–dynein-dynactin interaction does not need the C-terminal early endosome–binding site of HookA, and the cytosolic ΔC-HookA-GFP fusion pulls down dynein-dynactin effectively (Zhang *et al.*, 2014). Thus the pull-down experiments using the cytosolic ΔC-HookA-GFP allow us to determine whether VezA mediates the interaction between HookA and dynein-dynactin. Our Western analyses indicate that ΔC-HookA-GFP is able to pull down normal amounts of dynein, dynactin, and the dynein-binding protein NudF/LIS1 in the Δ*vezA* extract (Figure 5D). Thus VezA is not required for linking dynein-dynactin to the cytosolic ΔC-HookA. We next examined whether early endosome–bound, full-length HookA can pull down dynein and dynactin. For this experiment, we used strains containing HookA-GFP and HookA-GFP/Δ*vezA*, respectively. Because HookA-GFP is physically associated with early endosomes in the absence of VezA, it can be used to pull down early endosomes in the absence of detergent and allow us to determine whether dynein

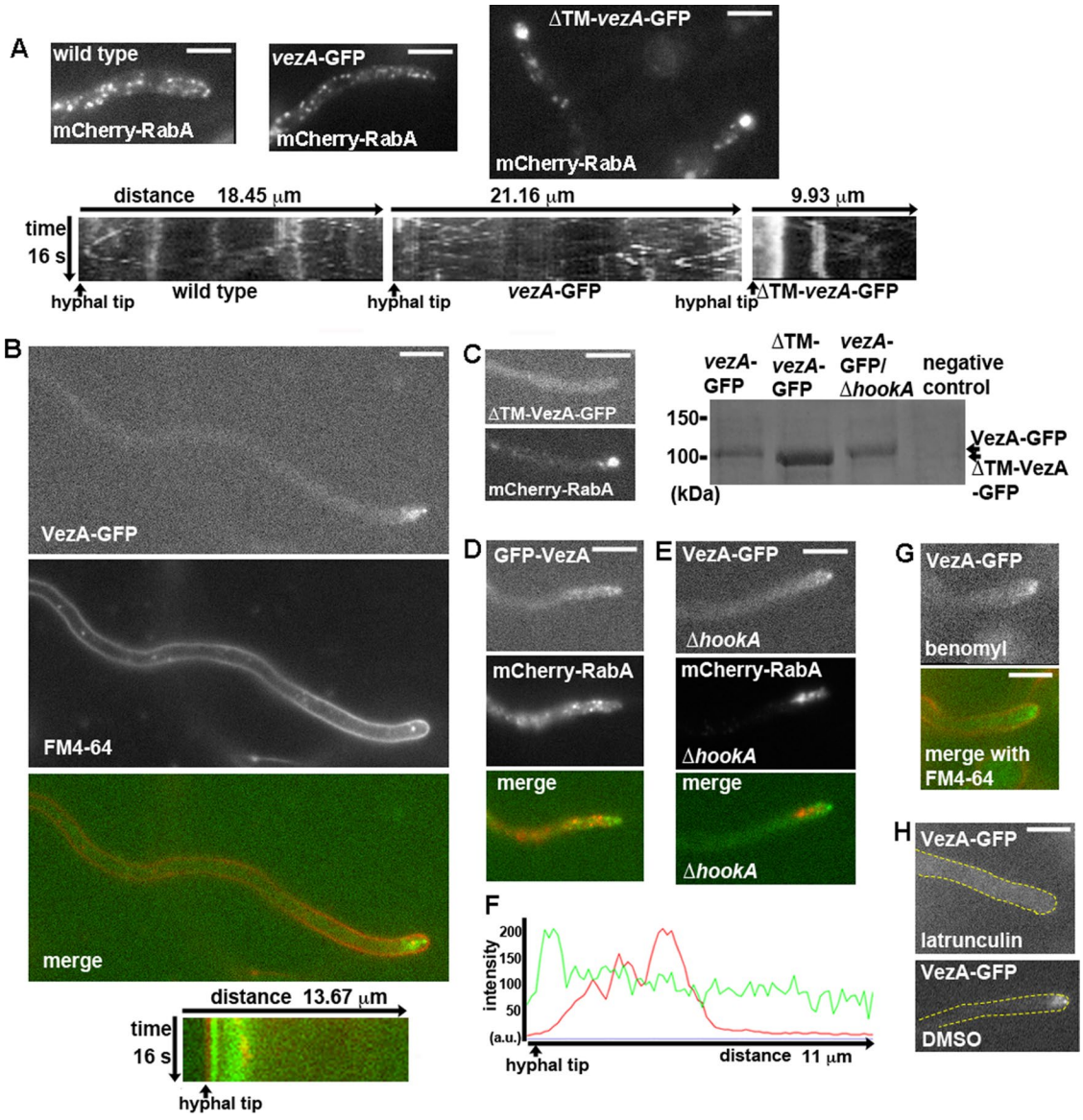

FIGURE 4: The functional VezA-GFP fusion proteins are concentrated at the hyphal tip. (A) The normal distribution of mCherry-RabA–labeled early endosomes in the *vezA*-GFP strain indicates that VezA-GFP is functional. In contrast, the ΔTM-*vezA*-GFP strain shows an abnormal accumulation of early endosomes at the hyphal tip, indicating that the predicted transmembrane domains are important for VezA function. Kymographs are shown below to indicate that early endosomes move normally in the wild-type and *vezA*-GFP strains but largely accumulate at the hyphal tip in the ΔTM-*vezA*-GFP strain. The images and kymographs are from Supplemental Movie S3 (mCherry-RabA in the wild-type control), Supplemental Movie S4 (mCherry-RabA in the *vezA*-GFP strain), and Supplemental Movie S5 (mCherry-RabA in the ΔTM-*vezA*-GFP strain). (B) Images of VezA-GFP and FM4-64 in the same hypha. Glucose-containing medium was used, which prevented the expression of the *alcA*-controlled mCherry-RabA. One kymograph is shown below to illustrate the hyphal-tip enrichment of the VezA-GFP signals. The merged image (green, VezA-GFP; red, FM4-64) and the kymograph below are from Supplemental Movie S6. Supplemental Movies S7 and S8 are provided to show two other examples of VezA-GFP accumulation at the hyphal tip. (C) Images of a ΔTM-VezA-GFP–containing hypha. Both GFP and the mCherry-RabA signals are shown for the same hypha. Right, Western blot showing that the ΔTM-VezA-GFP fusion proteins are stably expressed. (D) Images of GFP-VezA and mCherry-RabA in the same hypha. (E) Images of VezA-GFP and mCherry-RabA in the same Δ*hookA* mutant hypha. (F) A line scan of the merge image of E. (G) Images of a VezA-GFP–containing hypha cultured overnight in medium containing 1.2 μg/ml benomyl. (H) Images of a VezA-GFP–containing hypha treated with 100 μM latrunculin B (in DMSO) for 15 min and a control hypha treated in the same way but with DMSO only. Yellow dotted lines show the hyphal shape. Bars, 5 μm.

and dynactin are able to associate with HookA-bound early endosomes. Of interest, in this experiment, the amounts of pulled-down dynein, dynactin, and NudF/LIS1 are significantly reduced (Figure 5, E and F), indicating that dynein–early endosome interaction is defective. This result is consistent with the decrease in the frequency of dynein-mediated transport in the Δ*vezA* mutant (Figure 2E). Together the results obtained with ΔC-HookA and full-length HookA indicate that whereas VezA is required for regulating the interaction

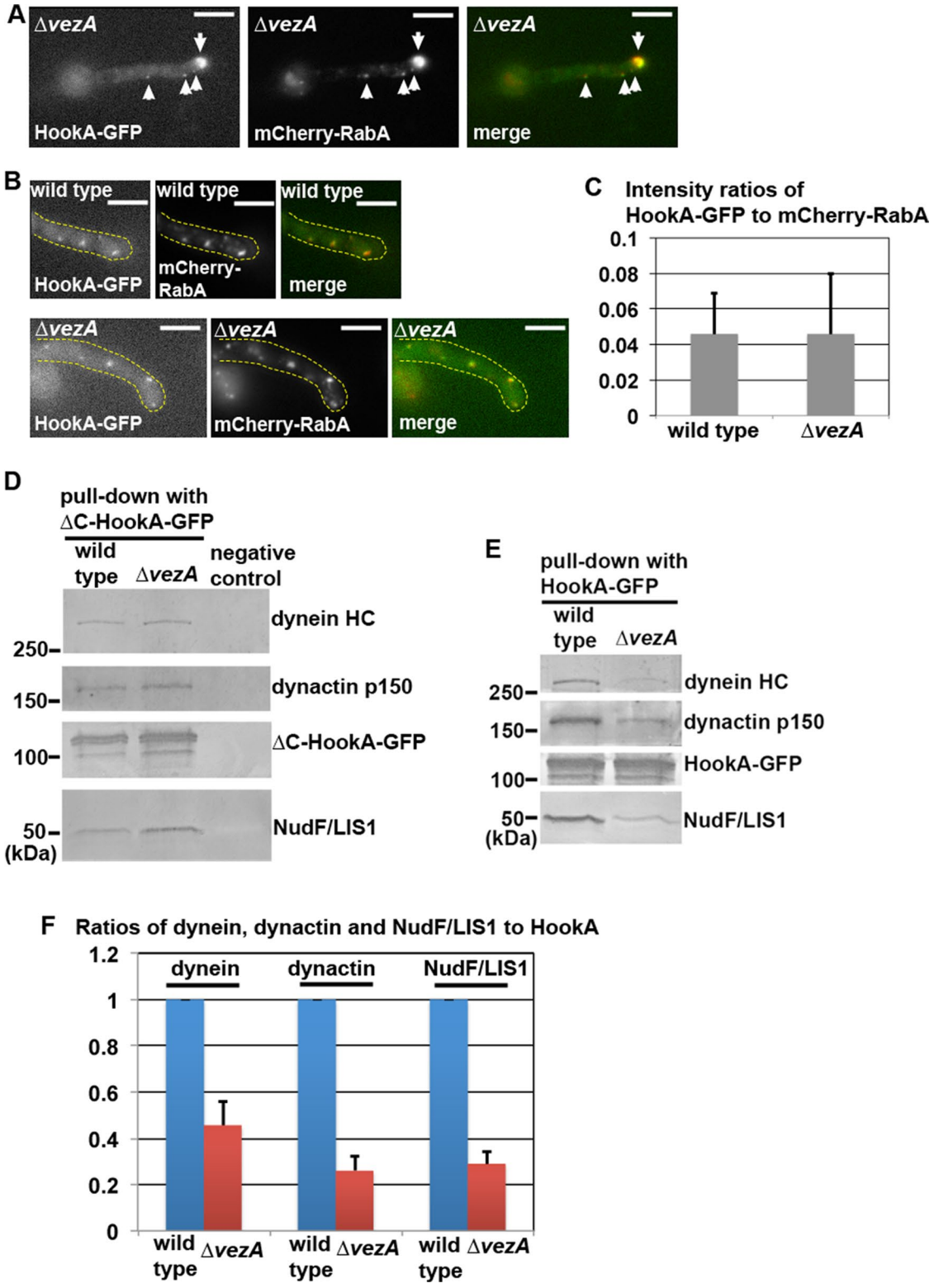

FIGURE 5: VezA does not affect HookA–early endosome association but affects the physical interaction between the early endosome–bound HookA and dynein-dynactin. (A) Localization of HookA-GFP in the Δ*vezA* mutant. HookA-GFP largely colocalizes with mCherry-RabA–labeled early endosomes at the hyphal tip in the Δ*vezA* mutant. Arrows indicate the hyphal tip area where both the GFP and mCherry signals accumulate and largely overlap. Arrowheads indicate the individual early endosomes with HookA-GFP. Bars, 5 μm. (B) HookA-GFP colocalizes with mCherry-RabA–labeled early endosomes in benomyl-treated wild-type and Δ*vezA* cells. Yellow dotted lines show the hyphal shape. Bars, 5 μm. (C) A quantitative analysis of the intensity ratios of HookA-GFP to mCherry-RabA in benomyl-treated wild-type and Δ*vezA* cells. The mean ± SD values are 0.0460 ± 0.0232 for wild type ($n = 20$) and 0.0456 ± 0.0339 for Δ*vezA* ($n = 20$), and the mean value of the mutant is not different from that of the wild type at $p = 0.05$. (D) Western analysis showing that VezA does

between early endosome–bound HookA and dynein-dynactin in vivo, it is unlikely to be required for physically bridging the interaction. Thus VezA is more likely a regulator than an additional cargo adapter.

DISCUSSION

The identification of VezA, a protein that localizes at the hyphal tip, for early endosome distribution clearly adds important conceptual complexity to our understanding of dynein-based transport: it suggests that dynein–cargo interaction in vivo requires novel factors beyond cargo adapters. However, although the localization of VezA at the hyphal tip region where microtubule plus ends are located is consistent with VezA being a positive regulator of the dynein–early endosome interaction, exactly how VezA regulates dynein–early endosome interaction needs to be studied further. The fungal hyphal-tip area is crowded with the actin cytoskeleton and many vesicles (Harris *et al.*, 2005; Steinberg, 2007; Fischer *et al.*, 2008; Schuster *et al.*, 2012; Pantazopoulou *et al.*, 2014; Riquelme and Sanchez-Leon, 2014; Zhu and Lee, 2014; Peñalva, 2015; Schultzhaus *et al.*, 2015), and VezA molecules are enriched at the hyphal-tip area in an actin-dependent manner. However, the latrunculin treatment that dispersed VezA within 15 min did not appear to affect significantly the frequency of dynein-mediated movement within 1 h (1.94 ± 0.998/16 s in latrunculin [$n = 31$] vs. 2.06 ± 1.03/16 s in dimethyl sulfoxide [DMSO; $n = 35$]). This result suggests that VezA may remain functional after it dissociates from the actin cytoskeleton at the hyphal tip. Alternatively, the cellular effect of VezA may be relatively long lasting, or VezA may only function in the context of the normal actin cytoskeleton at the hyphal tip.

Although some vesicles fully capable of binding dynein are more likely to be transported to the actin cytoskeleton after kinesin-mediated transport (Pantazopoulou *et al.*, 2014), as first shown in melanocytes (Wu *et al.*, 1998), early endosomes appear to be transported back directly by dynein. However, the directional switch from kinesin-3–mediated to dynein-mediated transport is not instant and may require complicated regulation (Bielska *et al.*, 2014). In *U. maydis*, before an early endosome binds dynein, half of the bound kinesin-3 molecules detach from it, whereas the number of bound Hook molecules remains constant (Bielska *et al.*, 2014). Whether this is functionally relevant remains to be determined, but given that fungal kinesin-3s contain a PH domain and other PH domain–containing kinesin-3s interact with phosphatidylinositol 4,5-bisphosphate (PIP2; Klopfenstein *et al.*, 2002; Klopfenstein and Vale, 2004), it is possible that the early endosome lipid composition may affect kinesin-3 binding (Bielska *et al.*, 2014), thereby affecting the direction switching process. Of interest, mammalian vezatin interacts specifically with the GTP-bound form (the active form) of Arf6 (Sanda *et al.*, 2010), which is known to activate the phosphatidylinositol 4-phosphate 5-kinase that generates PIP2 (Honda *et al.*, 1999; Brown *et al.*, 2001). Although the interaction with the GTP-bound Arf6 suggests that vezatin is an effector of Arf6 (Sanda *et al.*, 2010), the possibility that vezatin might negatively interfere with the function of active Arf6 is not completely excluded. Arf6 is involved in endocytosis and endocytic cargo sorting, and it is possibly in the same pathway as human Hook1 for endosome sorting of nonclathrin cargo (Donaldson, 2003; Maldonado-Baez *et al.*, 2013; Maldonado-Baez and Donaldson, 2013). Moreover, Arf6 has also been shown to interact with the scaffolding proteins on recycling endosomes, thereby affecting the switch between dynactin and kinesin-1 (Montagnac *et al.*, 2009). Future work is needed to address the possible interaction between VezA and the Arf6 homologue in *A. nidulans* (Lee *et al.*, 2008; Lee and Shaw, 2008).

The functional connection between vezatin and cytoplasmic dynein in higher eukaryotes has not been established. Vezatin in mammalian cells is considered to be a transmembrane protein, but its localization at the cell–cell contact sites is supported by the actin cytoskeleton (Kussel-Andermann *et al.*, 2000; Bahloul *et al.*, 2009), similar to the actin-dependent localization of VezA. Of interest, cytoplasmic dynein has also been found to localize to the cortex of the adherens junctions in an actin-dependent manner, although the function of dynein there has been implicated in tethering microtubules (Ligon *et al.*, 2001; Ligon and Holzbaur, 2007). Vezatin is expressed in neuronal cells and has been implicated in regulating dendritic morphology in hippocampal neurons (Sanda *et al.*, 2010; Danglot *et al.*, 2012). Cytoplasmic dynein is also important for dendritic morphogenesis in *Drosophila* dendritic arborization neurons via its function in transporting Rab5-positive early endosomes (Satoh *et al.*, 2008). However, vezatin has never been shown to be important for the movement of Rab5-positive early endosomes in mammalian cells. Based on the present study, it will be worthwhile to test whether vezatin is involved in dynein-mediated intracellular transport of membranous cargoes in higher eukaryotes.

MATERIALS AND METHODS

A. nidulans strains, media, and mutagenesis

A. nidulans strains used in this study are listed in Table 1. For biochemical experiments, yeast extract plus glucose plus uridine and uracil liquid medium or minimal plus fructose liquid medium plus supplements was used. UV mutagenesis on spores of *A. nidulans* strains was done as previously described (Willins *et al.*, 1995; Xiang *et al.*, 1999). For 4′,6-diamidino-2-phenylindole (DAPI) staining of nuclei, cells were incubated in liquid minimal medium containing 1% glycerol plus supplements overnight at 32°C. For live-cell imaging experiments, liquid minimal medium containing 1% glycerol plus supplements was used, and cells were cultured at 32°C overnight and observed at room temperature. For some experiments on VezA-GFP, liquid minimal medium containing 0.1% (wt/vol) glucose was used to incubate cells overnight at room temperature; under this condition, *alcA*-controlled mCherry-RabA is not expressed.

not affect ΔC-Hook–dynein-dynactin interaction. Normal amounts of the dynein HC, the p150 subunit of dynactin, and NudF/LIS1 (a dynein-binding protein) can be pulled down with ΔC-HookA-GFP in the Δ*vezA* mutant. The negative control for the pull-down assay is a strain without any GFP tag. (E) Western analysis showing that VezA affects the interaction between the early endosome–bound HookA and dynein-dynactin. The amounts of the dynein HC, the p150 subunit of dynactin, and NudF/LIS1 (a dynein-binding protein) pulled down with HookA-GFP are significantly lower in the Δ*vezA* mutant. (F) Quantitative analysis of the Western analysis shown in E. The ratio of pulled-down dynein HC, dynactin p150, or NudF/LIS1 to HookA-GFP was calculated. Values of all the mutants are relative to the wild-type values, which are set at 1. The mean ± SD values were calculated from three independent pull-down experiments and are 0.46 ± 0.10 for dynein HC, 0.26 ± 0.07 for dynactin p150, and 0.29 ± 0.06 for NudF/LIS1. For all dynein, dynactin, and NudF/LIS values, the difference between the wild type and the Δ*vezA* mutant is significant ($p < 0.05$). The differences among the mutant dynein, dynactin, and NudF/LIS1 values are not significantly different at $p = 0.05$.

Strain	Genotype	Source
RQ2	GFP-*nudA*^{HC}*; argB2::[argB*-alcAp*::mCherry-*RabA]; ΔnkuA::argB; pyrG89; pyroA4; yA2*	Qiu *et al*. (2013)
RQ54	*argB2::[argB*-alcAp*::mCherry-*RabA]; ΔnkuA::argB; pyrG89; pyroA4; wA2*	Qiu *et al*. (2013)
JZ498	*ΔhookA::AfpyrG; argB2::[argB*-alcAp*::mCherry-*RabA]; ΔnkuA::argB; pyrG89; pyroA4; wA2*	Zhang *et al*. (2014)
JZ500	*hookA*-GFP-*AfpyrG*; *argB2::[argB*-alcAp*::mCherry-*RabA]; ΔnkuA::argB; pyrG89; pyroA4; wA2*	Zhang *et al*. (2014)
SNZ9	*ΔuncA::pyroA4; pyrG89*	Zekert and Fischer (2009)
XX223	Δp25::A*fpyrG*; GFP-*nudA*^{HC}*; argB2::[argB*-alcAp*::mCherry-*RabA]*	Zhang *et al*. (2011)
XY105	*eedC27*; GFP-*nudA*^{HC}*; argB2::[argB*-alcAp*::mCherry-*RabA]; ΔnkuA::argB; pyrG89; pyroA4; yA2*	This work
XY136	*ΔvezA::AfpyrG*; GFP-*nudA*^{HC}*; argB2::[argB*-alcAp*::mCherry-*RabA]; ΔnkuA::argB; pyrG89; pyroA4; yA2*	This work
XY139	*ΔuncA::pyroA4;* GFP-*nudA*^{HC}*; argB2::[argB*-alcAp*::mCherry-*RabA]; pyrG89; ΔnkuA::argB?*	This work
XY144	*ΔvezA::AfpyrG*; HookA-GFP-A*fpyrG; argB2::[argB*-alcAp*::mCherry-*RabA]; pabaA1; pyroA4; pyrG89? ΔnkuA::argB?*	This work
XY140	*ΔvezA::AfpyrG*; *ΔuncA::pyroA4;* GFP-*nudA*^{HC}*; argB2::[argB*-alcAp*::mCherry-*RabA]; yA2*; *ΔnkuA::argB?*	This work
XY161	*ΔvezA::AfpyrG*; *ΔhookA*::A*fpyrG*; GFP-*nudA*^{HC}*; argB2::[argB*-alcAp*::mCherry-*RabA]; yA2*; *ΔnkuA::argB?*	This work
XY163	*vezA*-GFP-*AfpyrG; argB2::[argB*-alcAp*::mCherry-*RabA]; ΔnkuA::argB; pyrG89; pyroA4; wA2*	This work
XY165	*vezA*-GFP-*AfpyrG; ΔhookA::AfpyrG; argB2::[argB*-alcAp*::mCherry-*RabA]; ΔnkuA::argB?; pyrG89?*	This work
XY166	*ΔvezA::AfpyrG*; *ΔC-hookA*-GFP-*AfpyrG*; *argB2::[argB*-alcAp*::mCherry-*RabA]; ΔnkuA::argB?*	This work
XY167	*ΔTM-vezA*-GFP-*AfpyrG; argB2::[argB*-alcAp*::mCherry-*RabA]; ΔnkuA::argB; pyrG89; pyroA4; wA2*	This work
XY170	*ΔvezA::AfpyrG*; Δp25::*AfpyrG*; GFP-*nudA*^{HC}*; argB2::[argB*-alcAp*::mCherry-*RabA]; ΔnkuA::argB? pyrG89? yA2*	This work
XY171	*gpdA*^{mini}::GFP-*vezA; argB2::[argB*-alcAp*::mCherry-*RabA]; ΔnkuA::argB; pyroA4; wA2*	This work

Markers not confirmed are indicated by question marks.

TABLE 1: *A. nidulans* strains used in this study.

Live-cell imaging and analyses and drug treatments

Fluorescence microscopy of live *A. nidulans* hyphae was as described (Yao *et al*., 2014; Zhang *et al*., 2014). All images were captured at room temperature using an Olympus (Center Valley, PA) IX70 inverted fluorescence microscope linked to a PCO/Cooke Corporation (Romulus, MI) Sensicam QE cooled charge-coupled device camera. An UplanApo 100× objective lens (oil) with a 1.35 numerical aperture was used. A filter wheel system with GFP/mCherry-ET Sputtered series with high transmission (Biovision Technologies, Exton, PA) was used. IPLab software was used for image acquisition and analysis.

For most imaging experiments, the LabTek Chambered #1.0 borosilicate coverglass system from Nalge Nunc International (Rochester, NY) was used. For experiments with FM4-64 staining, we used Delta T dishes from Bioptechs (Butler, PA), which can be fixed on the Bioptechs heating stage so that the dish does not move during the addition of the dye. About 2 µl of FM4-64 (200 µM) was added to 1.2 ml of medium, and the cells were stained for ~1–5 min at room temperature. Because addition of the dye slightly disrupted the VezA-GFP signals, we took images of VezA-GFP first before adding the dye. Benomyl was used at the final concentration of 1.2 µg/ml, and latrunculin B (Sigma-Aldrich, St. Louis, MO) was used at the final concentration of 100 µM. For the short-time latrunculin B treatment, we followed a similar procedure to that described in Taheri-Talesh *et al*. (2008). Specifically, half of the culture medium was removed from the observation chamber to be mixed well with latrunculin and added back to the observation chamber. The solvent for latrunculin B, DMSO, was used as a control.

To quantitate the mCherry-RabA signals at hyphal tip, we chose a region of interest (ROI) covering an area from the hyphal apex to ~2 µm behind it and obtained the mean intensity value using IPLab software. To quantitate the signal intensity of HookA-GFP in relation to that of mCherry-RabA in benomyl-treated cells, we chose an ROI covering just the early endosome of interest and obtained the sum values of both GFP and mCherry signals using IPLab software. For each measurement, the exact same ROI box was dragged outside of the cell to take the background value, which was then subtracted from the sum value.

Construction of the Δ*vezA* mutant

For constructing the Δ*vezA* mutant, the following oligos were used to make the Δ*vezA* construct with the selective marker *pyrG* from *Aspergillus fumigatus*, *AfpyrG*, in the middle of the linear construct (Szewczyk *et al*., 2006): UUTRf (5′-AACAATCTTTGTCTCATCAATCAA-3′), UUTRr (5′-CTCGTAAACCAGGGATTCCATA-3′); FUSf (5′-TATGGAATCCCTGGTTTACGAGTGCTCTTCACCCTCTTCGCG-3′), FUSr (5′-GCTGAAGGATCAGAGGCTTGTCTGTCTGAGAGGAGGCACTG-3′); and UTRf (5′-ACAAGCCTCTGATCCTTCAGC-3′), UTRr (5′-AGTGCTCCTGGTCAATGTCCA-3′).

We then used two oligos, UUTRfi (5′-TGACGTCCCTAGTTGCCTGTA-3′) and UTRri (5′-AACGACATCAGGAGAGTCGTC-3′), for a fusion PCR to generate the Δ*vezA-AfpyrG* fragment that we used to transform into the wild-type strain RQ2. The strain containing the Δ*vezA* allele was confirmed by PCR of genomic DNA, and the primers used for verifying the correct integration were UUTRf and AfpyrG3 (5′-GTTGCCAGGTGAGGGTATTT-3′), and AfpyrG5 (5′-AGCAAAGTGGACTGATAGC-3′) and UTRr (Supplemental Figure S2).

Construction of the strain containing VezA-GFP

For constructing the VezA-GFP fusion, we first used the following oligos to amplify vezA genomic DNA and the GFP-*AfpyrG*

fusion from the plasmid pFNO3 (deposited in the Fungal Genetics Stock Center [sbs.umkc.edu/research_fungal_stock_center.cfm] by Stephen Osmani [Department of Molecular Genetics, The Ohio State University, Columbus, OH]; McCluskey *et al.*, 2010; Yang *et al.*, 2004): vgORFf (5′-TCGATGCTGCTGTGCTGTTGA-3′), vgORFr (5′-GAGGCTTGTGACGCGTTTTGA-3′); vgFUSf (5′-ATTCAAAACGCGTCACAAGCCTCGGAGCTGGTGCAGGCGCTGGAG-3′), vgFUSr (5′-TCAGAGGCTTGTGACGCGTTCTGTCTGAGAGGAGGCACTGATG-3′); vgUTRf (5′-TGATCCTTCAGCCACAGTCGA-3′), and UTRr (5′-AGTGCTCCTGGTCAATGTCCA-3′). We then used two oligos, vgORFfi (5′-CATACAGGAGGTGGAACTGGTA-3′) and UTRri (5′-AACGACATCAGGAGAGTCGTC-3′), for a fusion PCR to generate the VezA-GFP-A*fpyrG* fragment that we used to transform into a wild-type strain RQ54. The strain containing the *vezA*-GFP fusion gene integrated correctly at the *vezA* locus was confirmed by PCR of genomic DNA using primers vgORFf and UTRr.

Construction of the strain containing ΔTM-VezA-GFP

We made a ΔTM-*vezA*-GFP strain containing the ΔTM-*vezA*-GFP allele in the *vezA* locus, and in this strain, the two predicted transmembrane domains of VezA (Supplemental Figure S1) and the short stretch of amino acids in between are deleted and GFP is linked at the C-terminus of the mutant protein. The following oligos were used to make two fragments with the *vezA*-GFP genomic DNA as template: UUTRf (5′-AACAATCTTTGTCTCATCAATCAA-3′), dTMfuser (5′-CGTTGTAGATATTGCAGGAAGGT-3′), dTMfusef (5′-CTGACCTTCCTGCAATATCTACAACGAGACGCCAGTGGCTGAAATAC-3′), and UTRr (5′-AGTGCTCCTGGTCAATGTCCA-3′). UUTRfi (5′-TGACGTCCCTAGTTGCCTGTA-3′) and UTRri (5′-AACGACATCAGGAGAGTCGTC-3′) were used for fusion PCR to generate the ΔTM-*vezA*-GFP fragment that we used to transform into a wild-type strain RQ54. The strain containing the ΔTM-*vezA*-GFP mutant fusion gene integrated correctly at the *vezA* locus was confirmed by PCR of genomic DNA using primers UUTRf and gpdGVr (5′-ATTCGGATACGATGCGACGCA-3′) and also primers AfpyrG5 and UTRr.

Construction of the strain containing *gpdA*^{mini}::GFP-VezA

We made a strain containing the *gpdA*^{mini}::GFP-*vezA* allele in the *vezA* locus. In the *gpdA*^{mini}::GFP-*vezA* strain, GFP is fused to the N-terminus of VezA, and expression of the fusion gene is driven by the *gpdA*^{mini} promoter (Pantazopoulou and Peñalva, 2009). By using the DNA synthesis service of GenScript USA (Piscataway, NJ), we made an ~3.1-kb DNA fragment containing the 1-kb region before the start codon of VezA, followed by the 355–base pair *gpdA*^{mini} promoter, the 0.7-kb GFP gene, and the 1-kb region after the start codon of VezA. This ~3.1-kb fragment was amplified using primers gpdGVfi (5′-CAATTCAAGTGTCCCTGAGATC-3′) and gpdGVri (5′-TGCGTTGTACTGGGTTCTGGA-3′) and cotransformed into RQ54 with a 3-kb fragment containing the *A. nidulans pyrG* gene, which was amplified from wild-type genomic DNA using primers pyrGF (5′-CGCTATCACGCCATAGCTTA-3′) and pyrGR (5′-GGGCGAGGTCAGTAGAAACA-3′). The strain containing the *gpdA*^{mini}::GFP-*vezA* fusion that integrated correctly at the *vezA* locus was confirmed by PCR of genomic DNA using primers gpdGVf (5′-TGCTAGTCGAAGCATATGAGCA-3′) and gpdGVr (5′-ATTCGGATACGATGCGACGCA-3′).

Biochemical pull-down assays to examine the interactions between HookA and dynein-dynactin

The μMACS GFP-tagged protein isolation kit (Miltenyi Biotec, San Diego, CA) was used to determine whether GFP-tagged HookA or ΔC-HookA pulls down dynein and dynactin. This was done as described previously (Zhang *et al.*, 2014). Strains were grown overnight in yeast extract/glucose or minimal medium containing 0.4% fructose (wt/vol). About 0.4 g of hyphal mass was harvested from overnight culture for each sample, and cell extracts were prepared using a lysis buffer containing 50 mM Tris-HCl, pH 8.0, and 10 μg/ml a protease inhibitor cocktail (Sigma-Aldrich). Cell extracts were centrifuged at 8000 × *g* for 15 min and then 16,000 × *g* for 15 min at 4°C, and supernatant was used for the pull-down experiment. To pull down GFP-tagged protein, 25 μl of anti-GFP MicroBeads was added to the cell extracts for each sample and incubated at 4°C for 30 min. The MicroBeads/cell extract mixture was then applied to the μColumn, followed by gentle wash with the lysis buffer as used for protein extraction (Miltenyi Biotec). Preheated (95°C) SDS–PAGE sample buffer was used as elution buffer. Western analyses were performed using the alkaline phosphatase (AP) system, and blots were developed using AP color development reagents from Bio-Rad (Hercules, CA). Quantitation of the protein band intensity was done using IPLab software as described previously (Yao *et al.*, 2012; Qiu *et al.*, 2013). The intensity ratios of the pulled-down dynein HC, dynactin p150, or NudF/LIS1 to GFP-labeled HookA or ΔC-HookA proteins were calculated. The antibody against GFP was from Clontech (Mountain View, CA; polyclonal). The antibodies against dynein HC, dynactin p150, and NudF/LIS1 were described previously (Xiang *et al.*, 1995a,b; Zhang *et al.*, 2008).

ACKNOWLEDGMENTS

We thank J. Zhang, R. Qiu, and M. Peñalva for helpful discussions and for sharing strains and protocols. We thank J. Bonifacino, J. Donaldson, and R. Cox for helpful discussions, R. Fischer and B. Oakley for strains, the Fungal Genetics Stock Center for the pFNO3 plasmid, and S. Osmani for depositing it. This work was funded by National Institutes of Health Grant RO1 GM097580 (to X.X.) and a Uniformed Services University intramural grant (to X.X.). Services for primer synthesis and DNA sequencing were provided by the Biomedical Instrumentation Center of the Uniformed Services University.

REFERENCES

Abenza JF, Galindo A, Pantazopoulou A, Gil C, de los Rios V, Peñalva MA (2010). *Aspergillus* RabB Rab5 integrates acquisition of degradative identity with the long distance movement of early endosomes. Mol Biol Cell 21, 2756–2769.

Abenza JF, Pantazopoulou A, Rodriguez JM, Galindo A, Peñalva MA (2009). Long-distance movement of *Aspergillus nidulans* early endosomes on microtubule tracks. Traffic 10, 57–75.

Akhmanova A, Hammer JA 3rd (2010). Linking molecular motors to membrane cargo. Curr Opin Cell Biol 22, 479–487.

Araujo-Bazan L, Peñalva MA, Espeso EA (2008). Preferential localization of the endocytic internalization machinery to hyphal tips underlies polarization of the actin cytoskeleton in *Aspergillus nidulans*. Mol Microbiol 67, 891–905.

Bahloul A, Simmler MC, Michel V, Leibovici M, Perfettini I, Roux I, Weil D, Nouaille S, Zuo J, Zadro C, *et al.* (2009). Vezatin, an integral membrane protein of adherens junctions, is required for the sound resilience of cochlear hair cells. EMBO Mol Med 1, 125–138.

Basu R, Chang F (2011). Characterization of dip1p reveals a switch in Arp2/3-dependent actin assembly for fission yeast endocytosis. Curr Biol 21, 905–916.

Bielska E, Schuster M, Roger Y, Berepiki A, Soanes DM, Talbot NJ, Steinberg G (2014). Hook is an adapter that coordinates kinesin-3 and dynein cargo attachment on early endosomes. J Cell Biol 204, 989–1007.

Brown FD, Rozelle AL, Yin HL, Balla T, Donaldson JG (2001). Phosphatidylinositol 4,5-bisphosphate and Arf6-regulated membrane traffic. J Cell Biol 154, 1007–1017.

Danglot L, Freret T, Le Roux N, Narboux Neme N, Burgo A, Hyenne V, Roumier A, Contremoulins V, Dauphin F, Bizot JC, *et al*. (2012). Vezatin is essential for dendritic spine morphogenesis and functional synaptic maturation. J Neurosci 32, 9007–9022.

Donaldson JG (2003). Multiple roles for Arf6: sorting, structuring, signaling at the plasma membrane. J Biol Chem 278, 41573–41576.

Echauri-Espinosa RO, Callejas-Negrete OA, Roberson RW, Bartnicki-Garcia S, Mourino-Perez RR (2012). Coronin is a component of the endocytic collar of hyphae of *Neurospora crassa* and is necessary for normal growth and morphogenesis. PLoS One 7, e38237.

Eckley DM, Gill SR, Melkonian KA, Bingham JB, Goodson HV, Heuser JE, Schroer TA (1999). Analysis of dynactin subcomplexes reveals a novel actin-related protein associated with the arp1 minifilament pointed end. J Cell Biol 147, 307–320.

Efimov VP, Morris NR (2000). The LIS1-related NUDF protein of *Aspergillus nidulans* interacts with the coiled-coil domain of the NUDE/RO11 protein. J Cell Biol 150, 681–688.

Egan MJ, Tan K, Reck-Peterson SL (2012). Lis1 is an initiation factor for dynein-driven organelle transport. J Cell Biol 197, 971–982.

Engqvist-Goldstein AE, Drubin DG (2003). Actin assembly and endocytosis: from yeast to mammals. Annu Rev Cell Dev Biol 19, 287–332.

Fischer R, Zekert N, Takeshita N (2008). Polarized growth in fungi–interplay between the cytoskeleton, positional markers and membrane domains. Mol Microbiol 68, 813–826.

Fu MM, Holzbaur EL (2014). Integrated regulation of motor-driven organelle transport by scaffolding proteins. Trends Cell Biol 24, 564–574.

Gachet Y, Hyams JS (2005). Endocytosis in fission yeast is spatially associated with the actin cytoskeleton during polarised cell growth and cytokinesis. J Cell Sci 118, 4231–4242.

Galindo A, Calcagno-Pizarelli AM, Arst HN Jr, Peñalva MA (2012). An ordered pathway for the assembly of fungal ESCRT-containing ambient pH signalling complexes at the plasma membrane. J Cell Sci 125, 1784–1795.

Granger E, McNee G, Allan V, Woodman P (2014). The role of the cytoskeleton and molecular motors in endosomal dynamics. Semin Cell Dev Biol 31, 20–29.

Han G, Liu B, Zhang J, Zuo W, Morris NR, Xiang X (2001). The *Aspergillus* cytoplasmic dynein heavy chain and NUDF localize to microtubule ends and affect microtubule dynamics. Curr Biol 11, 719–724.

Harris SD, Read ND, Roberson RW, Shaw B, Seiler S, Plamann M, Momany M (2005). Polarisome meets spitzenkorper: microscopy, genetics, and genomics converge. Eukaryot Cell 4, 225–229.

Honda A, Nogami M, Yokozeki T, Yamazaki M, Nakamura H, Watanabe H, Kawamoto K, Nakayama K, Morris AJ, Frohman MA, Kanaho Y (1999). Phosphatidylinositol 4-phosphate 5-kinase alpha is a downstream effector of the small G protein ARF6 in membrane ruffle formation. Cell 99, 521–532.

Horio T, Oakley BR (2005). The role of microtubules in rapid hyphal tip growth of *Aspergillus nidulans*. Mol Biol Cell 16, 918–926.

Kardon JR, Vale RD (2009). Regulators of the cytoplasmic dynein motor. Nat Rev Mol Cell Biol 10, 854–865.

Kilaru S, Schuster M, Latz M, Guo M, Steinberg G (2015). Fluorescent markers of the endocytic pathway in *Zymoseptoria tritici*. Fungal Genet Biol 79, 150–157.

Klopfenstein DR, Tomishige M, Stuurman N, Vale RD (2002). Role of phosphatidylinositol(4,5)bisphosphate organization in membrane transport by the Unc104 kinesin motor. Cell 109, 347–358.

Klopfenstein DR, Vale RD (2004). The lipid binding pleckstrin homology domain in UNC-104 kinesin is necessary for synaptic vesicle transport in *Caenorhabditis elegans*. Mol Biol Cell 15, 3729–3739.

Kramer H, Phistry M (1996). Mutations in the *Drosophila* hook gene inhibit endocytosis of the boss transmembrane ligand into multivesicular bodies. J Cell Biol 133, 1205–1215.

Kussel-Andermann P, El-Amraoui A, Safieddine S, Nouaille S, Perfettini I, Lecuit M, Cossart P, Wolfrum U, Petit C (2000). Vezatin, a novel transmembrane protein, bridges myosin VIIA to the cadherin-catenins complex. EMBO J 19, 6020–6029.

Lee IH, Kumar S, Plamann M (2001). Null mutants of the *Neurospora* actin-related protein 1 pointed-end complex show distinct phenotypes. Mol Biol Cell 12, 2195–2206.

Lee SC, Schmidtke SN, Dangott LJ, Shaw BD (2008). *Aspergillus nidulans* ArfB plays a role in endocytosis and polarized growth. Eukaryot Cell 7, 1278–1288.

Lee SC, Shaw BD (2008). ArfB links protein lipidation and endocytosis to polarized growth of *Aspergillus nidulans*. Commun Integr Biol 1, 51–52.

Lenz JH, Schuchardt I, Straube A, Steinberg G (2006). A dynein loading zone for retrograde endosome motility at microtubule plus-ends. EMBO J 25, 2275–2286.

Ligon LA, Holzbaur EL (2007). Microtubules tethered at epithelial cell junctions by dynein facilitate efficient junction assembly. Traffic 8, 808–819.

Ligon LA, Karki S, Tokito M, Holzbaur EL (2001). Dynein binds to beta-catenin and may tether microtubules at adherens junctions. Nat Cell Biol 3, 913–917.

Maldonado-Baez L, Cole NB, Kramer H, Donaldson JG (2013). Microtubule-dependent endosomal sorting of clathrin-independent cargo by Hook1. J Cell Biol 201, 233–247.

Maldonado-Baez L, Donaldson JG (2013). Hook1, microtubules, and Rab22: mediators of selective sorting of clathrin-independent endocytic cargo proteins on endosomes. Bioarchitecture 3, 141–146.

McCluskey K, Wiest A, Plamann M (2010). The Fungal Genetics Stock Center: a repository for 50 years of fungal genetics research. J Biosci 35, 119–126.

Miao R, Guo X, Zhi Q, Shi Y, Li L, Mao X, Zhang L, Li C (2013). VEZT, a novel putative tumor suppressor, suppresses the growth and tumorigenicity of gastric cancer. PLoS One 8, e74409.

Michelot A, Costanzo M, Sarkeshik A, Boone C, Yates JR 3rd, Drubin DG (2010). Reconstitution and protein composition analysis of endocytic actin patches. Curr Biol 20, 1890–1899.

Montagnac G, Sibarita JB, Loubery S, Daviet L, Romao M, Raposo G, Chavrier P (2009). ARF6 Interacts with JIP4 to control a motor switch mechanism regulating endosome traffic in cytokinesis. Curr Biol 19, 184–195.

Mooren OL, Galletta BJ, Cooper JA (2012). Roles for actin assembly in endocytosis. Annu Rev Biochem 81, 661–686.

Pagliardini L, Gentilini D, Sanchez AM, Candiani M, Vigano P, Di Blasio AM (2015). Replication and meta-analysis of previous genome-wide association studies confirm vezatin as the locus with the strongest evidence for association with endometriosis. Hum Reprod 30, 987–993.

Pantazopoulou A, Peñalva MA (2009). Organization and dynamics of the *Aspergillus nidulans* Golgi during apical extension and mitosis. Mol Biol Cell 20, 4335–4347.

Pantazopoulou A, Pinar M, Xiang X, Peñalva MA (2014). Maturation of late Golgi cisternae into RabE(RAB11) exocytic post-Golgi carriers visualized in vivo. Mol Biol Cell 25, 2428–2443.

Peñalva MA (2005). Tracing the endocytic pathway of *Aspergillus nidulans* with FM4-64. Fungal Genet Biol 42, 963–975.

Peñalva MA (2010). Endocytosis in filamentous fungi: Cinderella gets her reward. Curr Opin Microbiol 13, 684–692.

Peñalva MA (2015). A lipid-managing program maintains a stout Spitzenkorper. Mol Microbiol 97, 1–6.

Perlson E, Maday S, Fu MM, Moughamian AJ, Holzbaur EL (2010). Retrograde axonal transport: pathways to cell death? Trends Neurosci 33, 335–344.

Qiu R, Zhang J, Xiang X (2013). Identification of a novel site in the tail of Dynein heavy chain important for Dynein function in vivo. J Biol Chem 288, 2271–2280.

Riquelme M, Sanchez-Leon E (2014). The Spitzenkorper: a choreographer of fungal growth and morphogenesis. Curr Opin Microbiol 20, 27–33.

Sanda M, Ohara N, Kamata A, Hara Y, Tamaki H, Sukegawa J, Yanagisawa T, Fukunaga K, Kondo H, Sakagami H (2010). Vezatin, a potential target for ADP-ribosylation factor 6, regulates the dendritic formation of hippocampal neurons. Neurosci Res 67, 126–136.

Satoh D, Sato D, Tsuyama T, Saito M, Ohkura H, Rolls MM, Ishikawa F, Uemura T (2008). Spatial control of branching within dendritic arbors by dynein-dependent transport of Rab5-endosomes. Nat Cell Biol 10, 1164–1171.

Schroer TA (2004). Dynactin. Annu Rev Cell Dev Biol 20, 759–779.

Schultzhaus Z, Yan H, Shaw BD (2015). *Aspergillus nidulans* flippase DnfA is cargo of the endocytic collar and plays complementary roles in growth and phosphatidylserine asymmetry with another flippase, DnfB. Mol Microbiol 97, 18–32.

Schuster M, Kilaru S, Ashwin P, Lin C, Severs NJ, Steinberg G (2011a). Controlled and stochastic retention concentrates dynein at microtubule ends to keep endosomes on track. EMBO J 30, 652–664.

Schuster M, Lipowsky R, Assmann MA, Lenz P, Steinberg G (2011b). Transient binding of dynein controls bidirectional long-range motility of early endosomes. Proc Natl Acad Sci USA 108, 3618–3623.

Schuster M, Treitschke S, Kilaru S, Molloy J, Harmer NJ, Steinberg G (2012). Myosin-5, kinesin-1 and myosin-17 cooperate in secretion of fungal chitin synthase. EMBO J 31, 214–227.

Sirotkin V, Berro J, Macmillan K, Zhao L, Pollard TD (2010). Quantitative analysis of the mechanism of endocytic actin patch assembly and disassembly in fission yeast. Mol Biol Cell 21, 2894–2904.
Sousa S, Cabanes D, El-Amraoui A, Petit C, Lecuit M, Cossart P (2004). Unconventional myosin VIIa and vezatin, two proteins crucial for *Listeria* entry into epithelial cells. J Cell Sci 117, 2121–2130.
Steinberg G (2007). Hyphal growth: a tale of motors, lipids, and the Spitzenkorper. Eukaryot Cell 6, 351–360.
Steinberg G (2014). Endocytosis and early endosome motility in filamentous fungi. Curr Opin Microbiol 20, 10–18.
Szewczyk E, Nayak T, Oakley CE, Edgerton H, Xiong Y, Taheri-Talesh N, Osmani SA, Oakley BR (2006). Fusion PCR and gene targeting in *Aspergillus nidulans*. Nat Protoc 1, 3111–3120.
Taheri-Talesh N, Horio T, Araujo-Bazan L, Dou X, Espeso EA, Peñalva MA, Osmani SA, Oakley BR (2008). The tip growth apparatus of *Aspergillus nidulans*. Mol Biol Cell 19, 1439–1449.
Upadhyay S, Shaw BD (2008). The role of actin, fimbrin and endocytosis in growth of hyphae in *Aspergillus nidulans*. Mol Microbiol 68, 690–705.
Vallee RB, McKenney RJ, Ori-McKenney KM (2012). Multiple modes of cytoplasmic dynein regulation. Nat Cell Biol 14, 224–230.
Wedlich-Soldner R, Straube A, Friedrich MW, Steinberg G (2002). A balance of KIF1A-like kinesin and dynein organizes early endosomes in the fungus *Ustilago maydis*. EMBO J 21, 2946–2957.
Willins DA, Xiang X, Morris NR (1995). An alpha tubulin mutation suppresses nuclear migration mutations in *Aspergillus nidulans*. Genetics 141, 1287–1298.
Wu X, Bowers B, Rao K, Wei Q, Hammer JA 3rd (1998). Visualization of melanosome dynamics within wild-type and dilute melanocytes suggests a paradigm for myosin V function In vivo. J Cell Biol 143, 1899–1918.
Xiang X, Osmani AH, Osmani SA, Xin M, Morris NR (1995a). NudF, a nuclear migration gene in *Aspergillus nidulans*, is similar to the human LIS-1 gene required for neuronal migration. Mol Biol Cell 6, 297–310.
Xiang X, Qiu R, Yao X, Arst HN Jr, Peñalva MA, Zhang J (2015). Cytoplasmic dynein and early endosome transport. Cell Mol Life Sci 72, 3267–3280.
Xiang X, Roghi C, Morris NR (1995b). Characterization and localization of the cytoplasmic dynein heavy chain in *Aspergillus nidulans*. Proc Natl Acad Sci USA 92, 9890–9894.
Xiang X, Zuo W, Efimov VP, Morris NR (1999). Isolation of a new set of *Aspergillus nidulans* mutants defective in nuclear migration. Curr Genet 35, 626–630.
Xu L, Sowa ME, Chen J, Li X, Gygi SP, Harper JW (2008). An FTS/Hook/p107(FHIP) complex interacts with and promotes endosomal clustering by the homotypic vacuolar protein sorting complex. Mol Biol Cell 19, 5059–5071.
Yang L, Ukil L, Osmani A, Nahm F, Davies J, De Souza CP, Dou X, Perez-Balaguer A, Osmani SA (2004). Rapid production of gene replacement constructs and generation of a green fluorescent protein-tagged centromeric marker in *Aspergillus nidulans*. Eukaryot Cell 3, 1359–1362.
Yao X, Wang X, Xiang X (2014). FHIP and FTS proteins are critical for dynein-mediated transport of early endosomes in *Aspergillus*. Mol Biol Cell 25, 2181–2189.
Yao X, Zhang J, Zhou H, Wang E, Xiang X (2012). In vivo roles of the basic domain of dynactin p150 in microtubule plus-end tracking and dynein function. Traffic 13, 375–387.
Yeh TY, Kowalska AK, Scipioni BR, Cheong FK, Zheng M, Derewenda U, Derewenda ZS, Schroer TA (2013). Dynactin helps target Polo-like kinase 1 to kinetochores via its left-handed beta-helical p27 subunit. EMBO J 32, 1023–1035.
Yeh TY, Quintyne NJ, Scipioni BR, Eckley DM, Schroer TA (2012). Dynactin's pointed-end complex is a cargo-targeting module. Mol Biol Cell 23, 3827–3837.
Zekert N, Fischer R (2009). The *Aspergillus nidulans* kinesin-3 UncA motor moves vesicles along a subpopulation of microtubules. Mol Biol Cell 20, 673–684.
Zhang J, Li S, Fischer R, Xiang X (2003). Accumulation of cytoplasmic dynein and dynactin at microtubule plus ends in *Aspergillus nidulans* is kinesin dependent. Mol Biol Cell 14, 1479–1488.
Zhang J, Qiu R, Arst HN Jr, Peñalva MA, Xiang X (2014). HookA is a novel dynein-early endosome linker critical for cargo movement in vivo. J Cell Biol 204, 1009–1026.
Zhang J, Wang L, Zhuang L, Huo L, Musa S, Li S, Xiang X (2008). Arp11 affects dynein-dynactin interaction and is essential for dynein function in *Aspergillus nidulans*. Traffic 9, 1073–1087.
Zhang J, Yao X, Fischer L, Abenza JF, Peñalva MA, Xiang X (2011). The p25 subunit of the dynactin complex is required for dynein-early endosome interaction. J Cell Biol 193, 1245–1255.
Zhang J, Zhuang L, Lee Y, Abenza JF, Peñalva MA, Xiang X (2010). The microtubule plus-end localization of *Aspergillus* dynein is important for dynein-early-endosome interaction but not for dynein ATPase activation. J Cell Sci 123, 3596–3604.
Zhu Y, Lee WL (2014). The role of +TIPs in directional tip expansion. Mol Microbiol 94, 486–489.